Lawrence Berkeley National Laboratory

Title
Performance of stainless steel interconnects with (Mn,Co)3O4-Based coating for solid oxide electrolysis

Permalink
https://escholarship.org/uc/item/33x843rk

Journal
International Journal of Hydrogen Energy, 47(58)

ISSN
0360-3199

Authors
Dogdibegovic, Emir
Ibanez, Sergio
Wallace, Anila
et al.

Publication Date
2022-07-01

DOI
10.1016/j.ijhydene.2022.05.206

Peer reviewed

Performance of Stainless Steel Interconnects with $(Mn,Co)_3O_4$-Based Coating

for Solid Oxide Electrolysis

Emir Dogdibegovic[1]*, Sergio Ibanez[1], Anila Wallace[1], David Kopechek[1], Gene Arkenberg[1], Scott Swartz[1], John M. Funk[1], Michael Reisert[2], Muhammad Anisur Rahman[2], Ashish Aphale[2], Prabhakar Singh[2], Hanping Ding[3], Wei Tang[3], Michael V. Glazoff[3], Dong Ding[3], Theis L. Skafte[4], and Michael C. Tucker[4]

1. Nexceris, 2. University of Connecticut, 3. Idaho National Laboratory, 4. Lawrence Berkeley National Laboratory

*e.dogdibegovic@nexceris.com

Abstract

Mixed transition-metal oxide coatings are commonly applied to stainless steel interconnects for solid oxide cell stacks. Such coatings reduce oxidation and Cr evaporation rates, leading to improved degradation rate and stack lifetime. Here, the ChromLok™ MCO-based composition $(Mn,Co)_3O_4$ is applied to Crofer 22 APU stainless steel and evaluated specifically for application in solid oxide electrolyzer stacks operating around 800°C and utilizing oxygen-ion-conducting solid oxide cells. The MCO coating is found to decrease the stainless steel oxidation rate by about one order of magnitude, and decrease the Cr evaporation rate by fourfold. The coating also dramatically lowers the rate of area-specific resistance increase for stainless steel coupons oxidized for 500 h with constant current applied, from 33 $m\Omega*cm^2$ kh^{-1} for an uncoated coupon to less than 4 $m\Omega*cm^2$ kh^{-1} for coated coupons. The coating is demonstrated on full-scale interconnects for single-cells, where the coating dramatically reduces degradation rate, and for a stack, which displays stable operation for 700 h.

Introduction

High temperature electrolysis (HTE) using solid oxide electrolysis cells (SOEC) is a very efficient method to produce hydrogen from steam, and is being developed and demonstrated globally as part of the hydrogen economy. SOEC cells typically comprise a Ni-based fuel electrode where steam is reduced to hydrogen, an yttria-stabilized zirconia (YSZ) electrolyte that conducts oxide ions from the steam/hydrogen (fuel) electrode to the oxygen electrode, and a metal oxide oxygen electrode where the oxygen is evolved into a sweep gas such as air. Multiple cells are assembled into a stack, which operates around 750 to 850°C. Individual cells are separated by interconnects, which are exposed to steam/hydrogen mixture on one side and oxygen (mixed with air or other sweep gas) on the other. The interconnects are typically made of stainless steel for reasons of cost, electronic conductivity, thermal expansion match with the cell, and formability into the shaped gas channels that deliver reactants to the whole area of the cell. It is widely recognized that the stainless steel must be coated on the air/oxygen side to reduce its oxidation rate and maintain low resistance and minimize Cr transport from the interconnect to the cell catalysts to avoid catalyst poisoning [1, 2]. Therefore, the performance of the interconnect coating and its behavior in the aggressive operating conditions are critical for the deployment of HTE technology.

The ChromLok^{TM} coating line produced by Nexceris includes a range of coating materials for stainless steel substrates. For the active area of the oxygen electrode-side interconnect surface, the ChromLok $(Mn,Co)_3O_4$ (MCO)-based composition is chosen for its oxidation resistance and high conductivity, which is critical for all components in the current path. ChromLok displayed stable area-specific resistance (ASR) for 35 kh in humidified air, relevant to solid oxide fuel cell (SOFC) operation [3]. Similar coating compositions have been demonstrated to significantly decrease the rate of stainless steel oxidation for SOFC conditions, compared to uncoated interconnect alloys [4-6]. MCO coatings reduce the oxidation rate

by acting as a barrier to diffusion of oxygen to the stainless steel surface [6]. Only a few studies of interconnect oxidation behavior specifically for the SOEC application with oxygen content higher than in air are reported, however [7-10]. The environment of the interconnect coating differs for SOEC operation compared to the well-studied SOFC situation: the current direction is reversed, the current density is generally higher than for SOFC, and the oxygen partial pressure is increased due to oxygen production at the oxygen electrode.

In this work, the suitability of MCO coated on Crofer 22 APU for use as an SOEC interconnect is assessed. This substrate alloy is chosen because it offers good oxidation resistance and Cr evaporation properties under solid oxide cell (SOC) operating conditions [9-11]. The impact of the MCO coating on oxidation rate is determined over a range of oxygen partial pressure and temperature relevant to SOEC operation. The coating is shown to dramatically reduce Cr transpiration both in ex-situ and single-cell experiments. The low and stable resistance of the coating is demonstrated over a wide range of current density and oxygen partial pressure. Stable operation of the MCO-coated interconnects is demonstrated in a stack operating in the SOEC mode. Finally, cost analysis indicates the coating can meet the cost target.

Experimental Methods

Sample preparation

Crofer 22 APU stainless steel sheets (0.3 mm thickness) were cut into 2 x 2 cm coupons. Pristine coupons were used for baseline studies. Commercial MCO powder was synthesized at Nexceris and milled to a particle size distribution resulting in 8 to 10 $m^2\,g^{-1}$ surface area, then used to make suspension for coating. Coupons were coated with MCO suspension using aerosol spray deposition. MCO was deposited on all four edges and both faces of the coupons to avoid excessive Cr evaporation from the uncoated edges, which can cause significant over-estimation of the Cr evaporation rate [12]. The coupons were then heat

treated through a reduction process followed by oxidation in air to form a conformal MCO coating with ~ 12 μm thickness, similar to previous studies [13-16]. For interconnectors used in stacks, only the oxygen electrode side was coated with the MCO coating. Quality control inspection (visual, cross-section imaging, and thickness measurement) was performed to ensure the applied coating meets the manufacturing standards.

Oxidation

Oxidation behavior of the specimens was evaluated at 800 and 850 °C. Coupons were placed in an alumina sample holder in a tube furnace which was calibrated to be less than 5 °C from the target temperature. Weight gain of the samples was determined every 100 h for up to 500 h using an analytical balance (Mettler Toledo XP205, precision of 0.01 mg). At least two identical samples were measured for each condition and weight gain values were averaged. Furnace heating and cooling rates were 5 °C/min. Samples were oxidized in 97% air/3% H_2O or 30% O_2/3% H_2O/67% N_2 mixtures to simulate the oxygen electrode environment. Humidity was introduced by bubbling the gases through a distilled water tank with the tank temperature maintained at room temperature.

Chromium transpiration experiments

Chromium transpiration experiments were designed to quantify chromium evaporation rates of coated and non-coated metallic samples under SOEC system operating conditions, and used an experimental setup that was described in detail previously [17, 18]. A single metal sample was placed within a quartz tube at the center of a tube furnace with air flowing at 300 standard cm^3 min^{-1}. The air was delivered through a water bubbler wrapped with heated tape to add 3% humidity. The tube furnace was heated at a rate of 5 °C min^{-1} to 800 °C and held for 500 h prior to cooling at 5 °C min^{-1}. The quartz tube within the furnace had a central capillary opening to prevent back diffusion of flowing gas. This tube was connected

to a quartz condenser tube using a quartz elbow. Vaporous Cr species condensed at the elbow, causing visual discoloration of the quartz and an indication of evaporated Cr. The condenser tube was attached to a chiller designed to promote condensation of Cr-containing water vapor, which was collected in a large collector flask. The flask was connected to a wash bottle to collect any remaining vaporous Cr.

Upon completion of the 500 h test, the sample was removed and the test reactor components including the reactor tube, elbow, condenser tube, collector flask, and wash bottle were collected for cleaning. An acidic solution (20% HNO_3) was added to the collector flask and wash bottle, while the tubing and elbow were submerged in the solution. The glassware was soaked in solution for at least 24 h to extract deposited Cr species. A basic permanganate/ hydroxide dilute solution (stirred and heated to 90 °C) was prepared and added to the glassware to remove remaining Cr species. Samples from the solution were analyzed using inductively-coupled plasma spectroscopy (ICP) and the measured Cr concentration was used to calculate the Cr evaporation rate.

Area-specific resistance measurements

Coupons were loaded in a quartz sample holder in a tube furnace (Lindberg) which was calibrated to be less than 5 °C from the target temperature. Pt wires were welded to Pt mesh and applied to coupons via Pt paste, then pre-fired at 1000 °C for 1 hour in air. Active area of the coupon was 4 cm^2. Two samples per stand were loaded. Area specific resistance (ASR) behavior of the specimens was evaluated at 800 and 850 °C in 97% air/3% H_2O or 30% O_2/3% H_2O/67% N_2 by applying current density of 1 or 2 A/cm^2 using a digital power supply (BK Precision). Four probe measurement was conducted using a Keithley 2700 Multimeter Data Acquisition System with continuous computer data logging. Humidity was introduced by bubbling the gases through a distilled water tank with the tank temperature maintained at room temperature.

Cell and stack testing and operation

Single electrolyte-supported full cells (25 cm^2 total area with 16 cm^2 electrode active area) and stacks (42 cm^2 electrode active area) with coated interconnector on the oxygen electrode side were mounted in a box furnace (Mellen) with 4-probe connections and sealing paste. A baseline cell with uncoated interconnector was used for comparison. A custom-built test apparatus with LabView code was used to control mass flow controllers (Alicat), digital power supply (TDK-Lambda), electronic load (Agilent N3300A), and multimeter and data acquisition system (Keithley 2700). The cells and stack were operated at nominally 800 °C with 75% steam and 25 % hydrogen in SOEC mode.

TEM and XRD analysis

The microscope used for milling and sample lift-out preparation was a Helios Nanolab 460F1 DualBeam (FEI, ThermoFisher Scientific). The transmission electron microscopy (TEM) system used to produce elemental mapping and high angle annular dark field (HAADF) imaging of FIB-prepared lift-out samples was a Talos F200S G2 TEM (FEI, ThermoFisher Scientific). X-ray diffraction (XRD) spectra were generated by a Bruker D5005 X-ray Diffractometer equipped with a Cu Kα X-ray source. Patterns were generated over a 2θ range of 20° − 80°.

SEM and EDS Analysis

The surface morphology and bulk structure of the oxide scales and coatings were examined using scanning electron microscopy (SEM, JEOL-7500F and Quanta 250 FEG, ThermoFisher Scientific) and energy dispersive X-ray spectroscopy (EDS, Thermo Scientific and AMETEK, Inc.).

Results and Discussion

Deposition and characterization of MCO coatings

The MCO coating is deposited as a powder by aerosol spraying, followed by a reduction-oxidation heat treatment. After this process is complete, the coating is approximately 12 μm thick and well-adhered to the Crofer 22 APU substrate, Fig 1. The MCO grain size is around 1 μm, and the residual pores on the surface are smaller than 3 μm. There is a clear gradient in porosity, with the outside surface of the coating having more residual porosity, and the porosity diminishing into the depth of the coating. At the coating/stainless steel interface the coating appears completely densified. A similar structure was observed previously for MCO coatings [4, 19]. This buried dense layer is expected to significantly increase the performance of the coating relative to a fully porous coating. There is a ~1 μm thick chromia scale at the surface of the stainless steel, which is formed during the coating heat treatment. It is anticipated that this thin scale is beneficial for oxidation resistance, as pre-oxidation to form a continuous conformal chromia scale is a common practice to improve oxidation resistance and prevent breakaway oxidation or corrosion over a wide variety of operating conditions [18, 20-24].
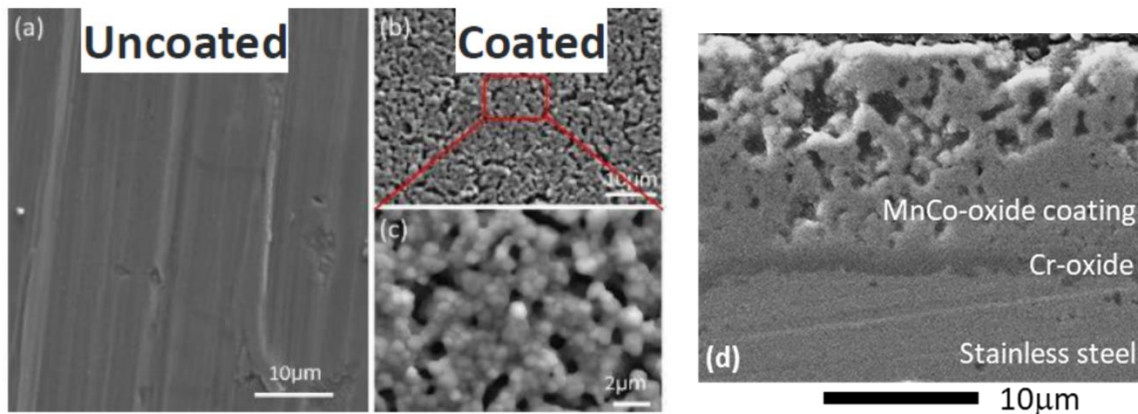

Figure 1. MCO coating structure. SEM images of (a) uncoated Crofer22APU surface, (b-c) MCO coated surface, and (d) cross-section of MCO coating and Crofer22APU substrate.

For ex-situ samples exposed entirely to oxidizing environment in this work (for oxidation, Cr transpiration, and ASR), the coating is applied to both faces and the edges of the stainless steel coupon. The coating is not necessary for the reducing environment of the H_2O/H_2 side of the interconnect, as pre-oxidation is sufficient to reduce the oxidation rate and curtail hydrogen cross-over [20]. Furthermore, the MCO composition partially reduces from the electronically conducting oxide to a mixture of Co and low-conductivity manganese oxide in the H_2O/H_2 environment, leading to increased electronic resistance.

Oxidation Studies

Oxidation resistance is the most important feature of a stainless steel interconnect for long-term performance in a SOEC stack. The oxidation behavior of coated and uncoated Crofer 22 APU alloy coupons was studied over a range of temperature and oxygen partial pressure, Fig 2. Weight gain due to oxidation was recorded every 100 h for 500 h in total, and follows the typical stainless steel oxidation behavior with an initial rapid weight gain (<100 h) followed by slower parabolic scale growth, Fig 2a. The parabolic oxidation rate constant was calculated from the weight gain data for 100 to 500 h, as commonly reported in the literature [9, 25-27]. The coating dramatically curtails oxidation at all conditions studied, reducing the oxidation rate constant by about one order of magnitude, Table 1. Stainless steel oxidation is controlled by oxygen diffusion through the chromia scale, which is highly thermally activated [27, 28]. Therefore, increasing the temperature from 800 to 850°C has a much larger impact than increasing the oxygen content of the atmosphere from 21% (air) to 30%. The oxidation rate constants are consistent with those reported in the literature for similar materials and conditions, Table 1 [9, 10, 25-27]. After 500 h of oxidation, the chromia scale and coating are still well adhered to the stainless steel alloy, Figs 2b-c. For the case of humidified 30% oxygen at 800°C, the scale thickness was 1.8 to 3.6 μm for the uncoated specimen (which had no scale before the oxidation experiment). The scale grew much less for the coated specimen, to 1.5 to 2.5 μm thick (starting from ~1 μm for the fresh coated specimen, Fig 1b).
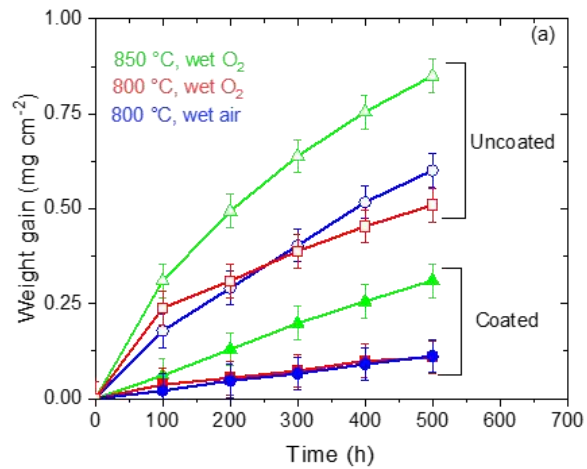
Figure 2. Oxidation behavior. (a) Intermittent weight gain data for coated (filled markers) and uncoated (open markers) coupons at 800 °C (circles, squares) or 850 °C (triangles) in humidified air (circles) or humidified O_2/N_2 (30:67) (squares). SEM cross section images of (b) coated and (c) uncoated samples after 500 h oxidation at 800 °C in humidified O_2/N_2 (30:67).

Table 1. Oxidation rates. Parabolic oxidation growth rate constants calculated from the data in Fig 2 compared for various conditions. Literature values for ferritic stainless steels are shown for comparison.

Reference		Atmosphere	Temperature (°C)	Oxidation Rate (10^{-14} g^2 cm^{-4} s^{-1})
This work	Uncoated	Wet air	800	7.6
		Wet 30% O2	800	4.4
		Wet 30% O2	850	20.9
	Coated	Wet air	800	0.8
		Wet 30% O2	800	0.6
		Wet 30% O2	850	2.96
[21]	Uncoated	Dry air	800	8.5
[10]	Uncoated	Ambient air	800	6
[10]	Coated	Ambient air	800	2.5
[12]	Uncoated	Wet air	800	5.4
[9]	Uncoated	Wet air	850	18.9
[23]	Uncoated	Wet air	850	20 to 33

Chromium Evaporation Studies

Migration of Cr from the interconnect to the oxygen electrode results in electrode poisoning [29, 30], and a key benefit of the MCO coating is reducing the Cr transport. Cr evaporation rate measurements in wet air at 800°C indicate a 4-fold reduction in Cr migration from the stainless steel when the coating is applied, Table 2. The values obtained here are similar to those reported in the literature, and the variation can be ascribed to different experimental conditions such as gas flow rate, humidity level, and sample temperature during the evaporation experiment [11, 31-33].

Table 2. Cr evaporation rates determined by transpiration experiments at 800°C in humidified air, and compared to literature values for Crofer 22 APU.

	Cr Evaporation Rate $(10^{-10}$ kg m^{-2} s$^{-1})$	
Reference	Uncoated	Coated
This work	1.1	0.25
[28]	3.5	-
[29]	3.0	-
[11]	1.7	0.1 to 0.6
[27]	5.0	0.2 to 0.5

After the evaporation exposure, the specimens were characterized further. For the uncoated coupon, the scale is a mixture of corundum-structure Cr_2O_3 and spinel-structure $(Mn,Cr)_3O_4$, Fig 3a. Note that the alloy contains Mn. TEM reveals that the coating microstructure remains relatively unchanged after 500 h, Fig 3b. The external area of the MCO layer is somewhat porous, the internal area is dense, and the grains are 1 to 3 μm, similar to the fresh sample (Fig 1). Cr accumulation is observed in the pores of the coating, which is consistent with gas-phase transport known to occur for Cr-oxide and Cr-oxyhydroxide [34, 35]. Some Si accumulation is also observed on the surface of the coating. It is not clear whether this Si arises from the stainless steel alloy (which contains up to 0.5% Si), coating processing, or glassware in the Cr evaporation experimental setup, and further effort is needed to determine the Si source. Future effort to increase the density throughout the whole coating thickness is anticipated to further decrease the Cr (and possibly Si) migration rate.
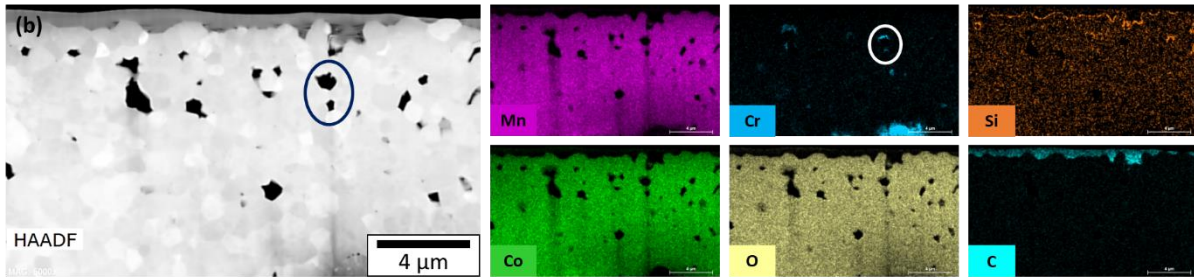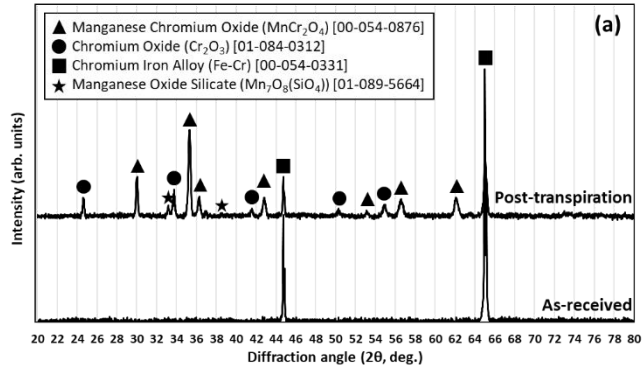
Figure 3. Post-transpiration analysis. (a) XRD patterns of the surface of uncoated Crofer22APU as received and after 500 h transpiration at 800°C in humidified air. (b) HAADF TEM cross section image and element maps of MCO coating after transpiration.

ASR Testing

Area-specific resistance (ASR) was determined for coated and uncoated stainless steel coupons over a range of temperature (800 to 850°C), pO_2 (21 to 30%), and current density (1 to 2 A cm^{-2}), Fig 4. The ASR arises from the electronic resistance of the stainless steel, oxidation scale, and coating layers. The stainless steel has a conductivity around 8.7 kS cm^{-1}, much higher than that of MCO (60 S cm^{-1}) or Cr_2O_3 (0.05 S cm^{-1}) [36-38]. The uncoated stainless steel therefore has the lowest initial ASR, as the coating has much lower conductivity than the bare metal and therefore dominates the total ASR. The coating and chromia scale dominate the initial ASR, and the contribution from the oxidation scale increases over time. The conductivities of the MCO coating and oxidation scale are thermally activated [37, 38], and the ASR at 850°C is clearly lower than at 800°C, despite some scatter in the initial ASR for various samples at 800°C

due to small variations in coating thickness, initial oxidation scale thickness, and alignment of the current collector pastes. There is no clear trend for the impact of pO_2 or current density on the initial ASR. While the initial ASR at 800°C is higher at 2 A cm^{-1} than at 1 A cm^{-1}, the opposite trend is observed at 800°C. Importantly, the ASR of the coated stainless steel is an order of magnitude lower than the cell ASR (~25 mΩ cm^2 at 800°C measured for a single cell), and therefore the interconnect resistance is expected to have a minimal impact on performance of the stack.
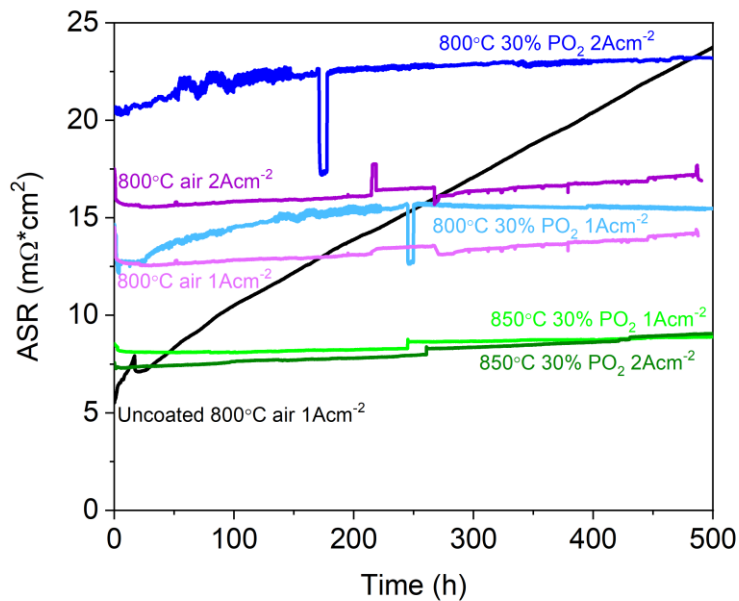
Figure 4. ASR stability. ASR for MCO-coated Crofer22APU during 500 h oxidation at 800 or 850 °C, in humidified air or O_2/N_2 (30:67), with 1 or 2 A cm^{-2} current density, and compared to uncoated Crofer22APU at 800 °C in humidified air at 1 A cm^{-2}.

Degradation of the ASR was monitored over 500 h with constant current density. Although the uncoated stainless steel displays the lowest initial ASR, its ASR increases dramatically over time at a degradation

rate of 33 mΩ cm^2 kh^{-1} and at 170 h surpasses that of the coated specimen operated at the same conditions (air, 1 A cm^{-2}, 800°C). The steady-state ASR degradation rate from 300 h (after initial transients) to the end of testing (~500 h) is approximately an order of magnitude lower for the coated samples than for the uncoated sample. For all of the coated samples, the ASR degradation rate is less than 4.5 mΩ cm^2 kh^{-1}. Compared to the impact of the coating, the impacts of increasing current density, pO$_2$, or temperature on the degradation rate are relatively small.

Electrochemical Testing

To clearly demonstrate the benefit of the MCO coating, cells were operated with uncoated and oxygen-electrode-side-coated interconnects, Fig 5a. Single cells (25 cm^2) were operated at 800°C with air as a sweep gas on the oxygen electrode side and 75:25 H$_2$O:H$_2$ on the fuel electrode side. For the uncoated interconnect, there was a rapid and large increase in the operating voltage (decrease in performance) over the first 150 h of operation, followed by moderate but continuous degradation. After operation, Cr was observed by SEM/EDS (not shown) in the oxygen electrode active layer (4 at% Cr) and current collector paste layer (15 at% Cr). Based on the ASR results above, we also assume that rapid Cr-scale growth on the interconnect contributed to the cell performance degradation. In contrast, with the MCO coating, extremely stable operation was observed for 440 h. After testing, the interconnect was analyzed with SEM/EDS, Fig 6. The coating is intact, with similar microstructure to the fresh coating, and a thin uniform Cr-scale layer at the interface between the alloy and MCO coating. Cr was not detected in the cell oxygen electrode active layer or current collector paste. Clearly, the MCO coating greatly improves the performance of the cell/interconnect assembly.
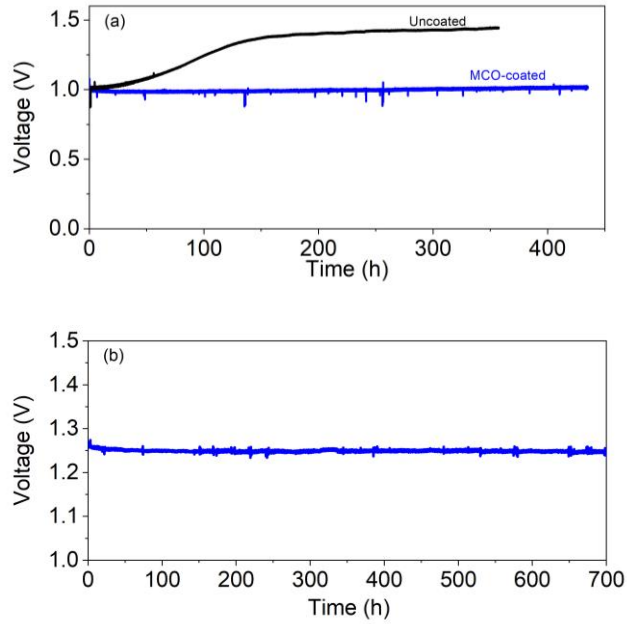
Figure 5. Validation of coating in operating cell and stack configurations. Operation was at 800 °C with air as sweep gas and steam/hydrogen (75:25) (theoretical OCV is 0.91 V). (a) Durability of a single 25 cm^2 cell at 0.2 A cm^{-2} with an MCO-coated (blue) or uncoated (black) Crofer22APU interconnect contacting the oxygen electrode. (b) Durability of a SOEC stack at 0.6 A cm^{-2} with 42 cm^2 active area and interconnects coated with MCO on the oxygen side.
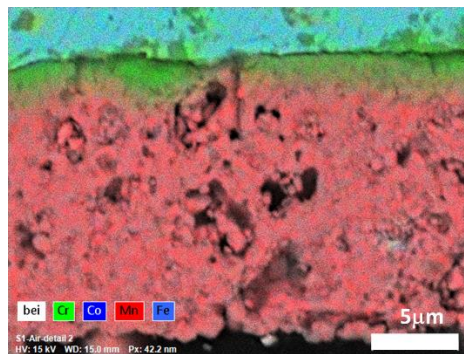

Figure 6. MCO coating after operation for 440 h in contact with a single cell.

Based on these promising single-cell testing results, a short stack was fabricated with 5 single cells (42 cm^2) and interconnects coated with MCO on the oxygen side. The stack was operated at 0.6 A cm^{-2} at nominally 800°C, with air as sweep gas on the oxygen side and 75:25 H$_2$O:H$_2$ on the fuel electrode side, Fig 5b. The initial voltage was 1.26 V, and the performance improved slightly during the initial 200 h break-in period. The 5-cell stack was operated for an additional 500 h, during which very stable operation was achieved with the performance slightly improving at a rate of 1.5 mV kh^{-1}. These results demonstrate the utility of the MCO coating as a critical part of the interconnect component in low-degradation SOEC stacks.

Conclusions

ChromLok MCO coating for the oxidizing side of solid oxide cell interconnects was studied over a range of temperature (800 to 850°C), pO$_2$ (21 to 30%), and current density (1 to 2 A cm^{-2}). The coating dramatically reduces oxidation, chromium transpiration, and ASR degradation rates at all conditions studied. This is similar to the performance in SOFC conditions, and the present detailed study in SOEC conditions significantly reduces the risk associated with translating this coating technology from SOFC development to SOEC deployment. The coating reduces the oxidation and ASR degradation rates by about one order of magnitude and reduces the Cr evaporation rate roughly 4-fold. Increasing the temperature from 800 to 850°C increases the oxidation rate roughly 5 times. Stable operation is achieved with no coating on the steam/hydrogen side. Future optimization of the coating preparation to increase density is expected to further reduce oxidation and Cr transpiration rates.

After assessing the coating performance and interconnect behavior ex-situ, coated interconnects were demonstrated with single solid oxide electrolysis cells and a stack of cells operating in electrolysis mode. The coating had a dramatic impact on the stability of single cells. Stable performance was obtained with a coated interconnect, whereas an uncoated interconnect caused rapid degradation of the cell

performance. Excellent stability was also observed for a multi-cell stack with coated interconnects, operating over 700 h at moderate current density.

References

[1] Mah JCW, Muchtar A, Somalu MR, Ghazali MJ. Metallic interconnects for solid oxide fuel cell: A review on protective coating and deposition techniques. International Journal of Hydrogen Energy. 2017;42:9219-29.
[2] Zhou L, Mason JH, Li W, Liu X. Comprehensive review of chromium deposition and poisoning of solid oxide fuel cells (SOFCs) cathode materials. Renewable and Sustainable Energy Reviews. 2020;134:110320.
[3] https://fuelcellmaterials.com/solutions/coatings/, accessed 3/17/2022

[4] Choi JP, Stevenson JW. Electrically Conductive and Protective Coating for Planar SOFC Stacks. ECS Transactions. 2017;78:1633-40.

[5] Larring Y, Norby T. Spinel and Perovskite Functional Layers Between Plansee Metallic Interconnect (Cr-5 wt % Fe-1 wt % Y$_2$O$_3$) and Ceramic (La$_{0.85}$Sr$_{0.15}$)$_{0.91}$MnO$_3$ Cathode Materials for Solid Oxide Fuel Cells. Journal of The Electrochemical Society. 2000;147:3251.

[6] Yang Z, Xia G, Simner SP, Stevenson JW. Thermal Growth and Performance of Manganese Cobaltite Spinel Protection Layers on Ferritic Stainless Steel SOFC Interconnects. Journal of The Electrochemical Society. 2005;152:A1896.

[7] Alnegren P, Froitzheim J, Svensson JE. Degradation of Ferritic Steel Interconnects in SOEC Environments. ECS Transactions. 2013;57:2261-70.

[8] Ardigo MR, Popa I, Chevalier S, Parry V, Galerie A, Girardon P, et al. Effect of Coatings on a Commercial Stainless Steel for SOEC Interconnect Application in Anode Atmosphere. ECS Transactions. 2013;57:2301-11.

[9] Palcut M, Mikkelsen L, Neufeld K, Chen M, Knibbe R, Hendriksen PV. Corrosion stability of ferritic stainless steels for solid oxide electrolyser cell interconnects. Corrosion Science. 2010;52:3309-20.

[10] Molin S, Chen M, Bentzen JJ, Hendriksen PV. High Temperature Oxidation of Ferritic Steels for Solid Oxide Electrolysis Stacks. ECS Transactions. 2013;50:11-20.

[11] Trebbels R, Markus T, Singheiser L. Reduction of Chromium Evaporation with Manganese-based Coatings. ECS Transactions. 2019;25:1417-22.

[12] Reddy MJ, Svensson J-E, Froitzheim J. Reevaluating the Cr Evaporation Characteristics of Ce/Co Coatings for Interconnect Applications. ECS Transactions. 2021;103:1899-905.

[13] Abdoli H, Molin S, Farnoush H. Effect of interconnect coating procedure on solid oxide fuel cell performance. Materials Letters. 2020;259:126898.

[14] Hu Y-Z, Yao S-W, Li C-X, Li C-J, Zhang S-L. Influence of pre-reduction on microstructure homogeneity and electrical properties of APS Mn1.5Co1.5O4 coatings for SOFC interconnects. International Journal of Hydrogen Energy. 2017;42:27241-53.

[15] Magdefrau NJ, Chen L, Sun EY, Yamanis J, Aindow M. Formation of spinel reaction layers in manganese cobaltite – coated Crofer22 APU for solid oxide fuel cell interconnects. Journal of Power Sources. 2013;227:318-26.

[16] Park B-K, Lee J-W, Lee S-B, Lim T-H, Park S-J, Park C-O, et al. Cu- and Ni-doped Mn1.5Co1.5O4 spinel coatings on metallic interconnects for solid oxide fuel cells. International Journal of Hydrogen Energy. 2013;38:12043-50.

[17] Aphale AN, Hu B, Reisert M, Pandey A, Singh P. Oxidation Behavior and Chromium Evaporation From Fe and Ni Base Alloys Under SOFC Systems Operation Conditions. JOM. 2019;71:116-23.

[18] Reisert M, Berova V, Aphale A, Singh P, Tucker MC. Oxidation of porous stainless steel supports for metal-supported solid oxide fuel cells. International Journal of Hydrogen Energy. 2020;45:30882-97.

[19] Wang R, Sun Z, Choi J-P, Basu SN, Stevenson JW, Tucker MC. Ferritic stainless steel interconnects for protonic ceramic electrochemical cell stacks: Oxidation behavior and protective coatings. International Journal of Hydrogen Energy. 2019;44:25297-309.

[20] Goebel C, Alnegren P, Faust R, Svensson J-E, Froitzheim J. The effect of pre-oxidation parameters on the corrosion behavior of AISI 441 in dual atmosphere. International Journal of Hydrogen Energy. 2018;43:14665-74.

[21] Alnegren P, Sattari M, Svensson J-E, Froitzheim J. Temperature dependence of corrosion of ferritic stainless steel in dual atmosphere at 600–800 °C. Journal of Power Sources. 2018;392:129-38.

[22] Gunduz KO, Chyrkin A, Goebel C, Hansen L, Hjorth O, Svensson J-E, et al. The effect of hydrogen on the breakdown of the protective oxide scale in solid oxide fuel cell interconnects. Corrosion Science. 2021;179:109112.

[23] Amendola R, Gannon P, Ellingwood B, Hoyt K, Piccardo P, Genocchio P. Oxidation behavior of coated and preoxidized ferritic steel in single and dual atmosphere exposures at 800°C. Surface and Coatings Technology. 2012;206:2173-80.

[24] Viklund P, Pettersson R. HCl-Induced High Temperature Corrosion of Stainless Steels in Thermal Cycling Conditions and the Effect of Preoxidation. Oxidation of Metals. 2011;76:111-26.

[25] Fu CJ, Sun KN, Zhang NQ, Chen XB, Zhou DR. Evaluation of lanthanum ferrite coated interconnect for intermediate temperature solid oxide fuel cells. Thin Solid Films. 2008;516:1857-63.

[26] Skilbred AWB, Haugsrud R. Sandvik Sanergy HT – A potential interconnect material for LaNbO4-based proton ceramic fuel cells. Journal of Power Sources. 2012;206:70-6.

[27] Falk-Windisch H, Svensson JE, Froitzheim J. The effect of temperature on chromium vaporization and oxide scale growth on interconnect steels for Solid Oxide Fuel Cells. Journal of Power Sources. 2015;287:25-35.

[28] Karczewski J, Brylewski T, Miruszewski T, Andersen KB, Jasinski PZ, Molin S. High-temperature kinetics study of 430L steel powder oxidized in air at 600–850 °C. Corrosion Science. 2019;149:100-7.

[29] Chen K, Hyodo J, Dodd A, Ai N, Ishihara T, Jian L, et al. Chromium deposition and poisoning of La0.8Sr0.2MnO3 oxygen electrodes of solid oxide electrolysis cells. Faraday Discussions. 2015;182:457-76.

[30] Wei B, Chen K, Zhao L, Lü Z, Ping Jiang S. Chromium deposition and poisoning at La0.6Sr0.4Co0.2Fe0.8O3−δ oxygen electrodes of solid oxide electrolysis cells. Physical Chemistry Chemical Physics. 2015;17:1601-9.

[31] Talic B, Falk-Windisch H, Venkatachalam V, Hendriksen PV, Wiik K, Lein HL. Effect of coating density on oxidation resistance and Cr vaporization from solid oxide fuel cell interconnects. Journal of Power Sources. 2017;354:57-67.

[32] Casteel M, Lewis D, Renko A, Willette P. Characterization of Vaporization Rates on SOFC Interconnect Alloys. ECS Transactions. 2019;35:2601-7.

[33] Stanislowski M, Froitzheim J, Niewolak L, Quadakkers WJ, Hilpert K, Markus T, et al. Reduction of chromium vaporization from SOFC interconnectors by highly effective coatings. Journal of Power Sources. 2007;164:578-89.

[34] Hilpert K, Das D, Miller M, Peck DH, Weiß R. Chromium Vapor Species over Solid Oxide Fuel Cell Interconnect Materials and Their Potential for Degradation Processes. Journal of The Electrochemical Society. 1996;143:3642-7.

[35] Ebbinghaus BB. Thermodynamics of gas phase chromium species: The chromium oxides, the chromium oxyhydroxides, and volatility calculations in waste incineration processes. Combustion and Flame. 1993;93:119-37.

[36] VDM Crofer 22 APU specification sheet, accessed 3/17/2022, https://www.vdm-metals.com/fileadmin/user_upload/Downloads/Data_Sheets/Data_Sheet_VDM_Crofer_22_APU.pdf

[37] Holt A, Kofstad P. Electrical conductivity and defect structure of Cr2O3. II. Reduced temperatures (<~1000°C). Solid State Ionics. 1994;69:137-43.

[38] Yang Z, Xia G-G, Li X-H, Stevenson JW. (Mn,Co)3O4 spinel coatings on ferritic stainless steels for SOFC interconnect applications. International Journal of Hydrogen Energy. 2007;32:3648-54.